Supplementary Materials for Crompton, Flowers and Dyck (2019). Glacial silt and clay, *Annals of Glaciology*

November 19, 2019

Contents

1 Fourier shape analysis

1.1 Spectral decomposition of shape

A time series $y(t)$ can be broken down into a linear combination of k components (x_k), whereby each component is the sum of sine and cosine waves with amplitude A and frequency f as

$$y(t) = \sum_{k=1}^{n} A_k \sin(2\pi f_k t) + B_k \cos(2\pi f_k t), \tag{1.1}$$

where there are n modes of k. In a Fourier grain analysis, the grain perimeter is transformed to radius–angle space such that $y(t) \rightarrow r(\theta)$. By computing the amplitude coefficients, we can eliminate

all high frequency components then recalculate a smoothed version of the grain shape that does not include high frequency undulations. We refer to this as the Fourier smoothed perimeter, and using this value, we can get an estimate of the grain roughness. The amplitude coefficients of the first k harmonics of the grain radius–angle waveform are computed in Matlab using the *fft* function. We use a Heaviside step function to discard higher harmonic components, then recompute a smoothed version of the radius–angle waveform using the Matlab *ifft* function. Other smoothing functions (spline, weighted moving average) could be appropriate alternatives.

In the main text we quantify perimeter roughness based on an analysis of the perimeter of convex hull. Whether the convex hull or Fourier roughness is more appropriate depends on the scale of roughness being analysed. For example, a concavity within a grain might be smoothed by abrasion which would be captured by the Fourier roughness but not by the convex hull roughness.

Convexities in the perimeter can result in double-valued radii for a given angle, complicating the computation of a Fourier transform. To eliminate convexities that lead to double-valued radii, we interpolate between the maximum of the double-valued points to a neighbouring point at the next greatest angle, then recompute the centre of mass and repeat the process. Less than 2% of the grains yield double-valued radii, and interpolating over the convexities has an insignificant effect on the results.

A similar and commonly used analysis is to take the Fourier power spectrum summed over a given range of harmonics as a measure of roughness (e.g. Dowdeswell, 1982; Gomez and others, 1988; Mazzullo and Ritter, 1991; Whalley, 1978). In an analysis of glacier sediment and source rock, Whalley (1978) suggests that the first four harmonics of the Fourier spectrum are thought to represent shape while the latter (4–20) are thought to represent roughness. Mazzullo and Ritter (1991) infer that the second normalized harmonic agrees well with Rittenhouse sphericity, while the nineteenth harmonic agrees well with the Krumbein roundness. We explore the use of the first k harmonics, but we find that the first five harmonics are best suited for this analysis.

Roughness values from the convex hull method are compared to those estimated using the Fourier-based method. To map the Fourier roughness onto an equivalent amount of edge abrasion, we calculate changes in roughness for thousands of synthetic elliptical grains. For each grain, boundary pixels with a length of $0.66\,\mu$m are randomly added or removed such that the area is preserved. We measure the change in the Fourier perimeter to derive an empirical relationship between the Fourier roughness and the number of pixels removed. We also test the extent to which the Fourier roughness depends on the predefined diameter and aspect ratio of the grain. This Monte-Carlo-type simulation provides a better sense of the minimum grain size appropriate for estimating edge abrasion.

1.2 Results

At each grain size that we simulate, the Fourier ratio decreases approximately linearly with the number of edge pixels being added/removed with a slope $m(D_i)$. The slope linearly increases with the grain size above $\sim 6\,\mu$m, but there is no correlation between size and slope below (Fig. 1.1). We therefore limit our use of both shape methods to inferring changes in roughness for grains larger than $6\,\mu$m. This limit is based on a pixel resolution of 0.66μm.

Results from both the Fourier and convex hull methods show that the extent of rounding is greatest for plagioclase (Fig. 1.2). For the Fourier method, quartz, plagioclase and carbonate initially increase in rounding with size but show less dependence at the largest grain sizes, while biotite increases in rounding for all grain sizes. Muscovite shows an increase in rounding at the smallest and largest grain sizes, with a minimum at intermediate grain sizes. Results from the convex hull method show a maximum increase in rounding at the boundary between very-fine silt and fine silt. Unlike the $\psi_j(D_i)$ and $f_j^A(D_i)$ distributions, the extent of rounding cannot simply be explained by the Moh's scale hardness.

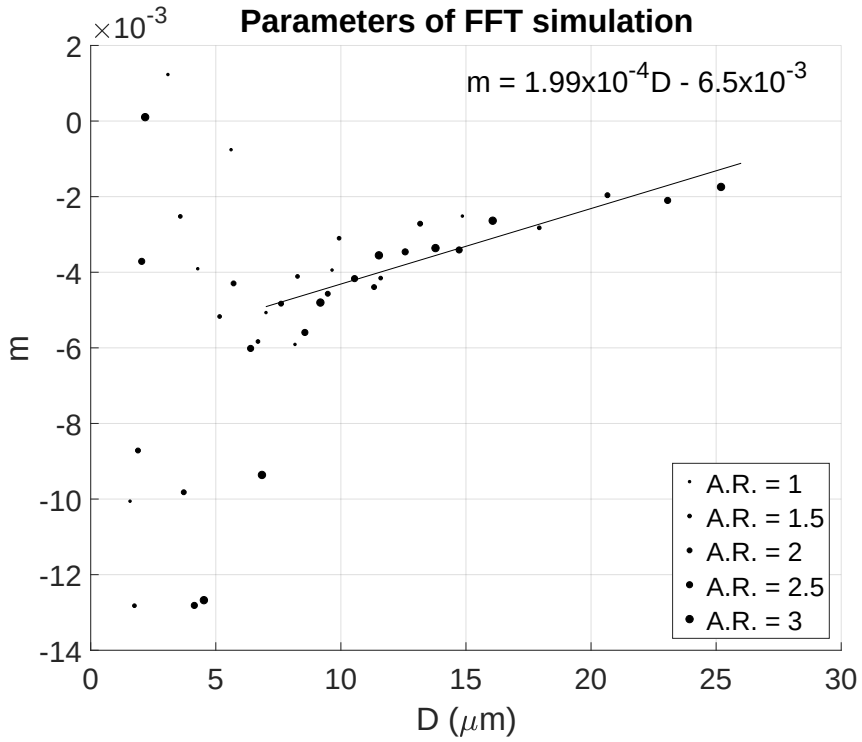

Figure 1.1: Parameters from the FFT simulations of grain roughness used to compute that change in area percent inferred from abrasion (Fig. 1.2). The slope m on the y-axis is computed from the number of pixels added/removed versus the grain size (D) for a given roughness, which was measured at various aspect ratios as denoted by the shapes of symbols.

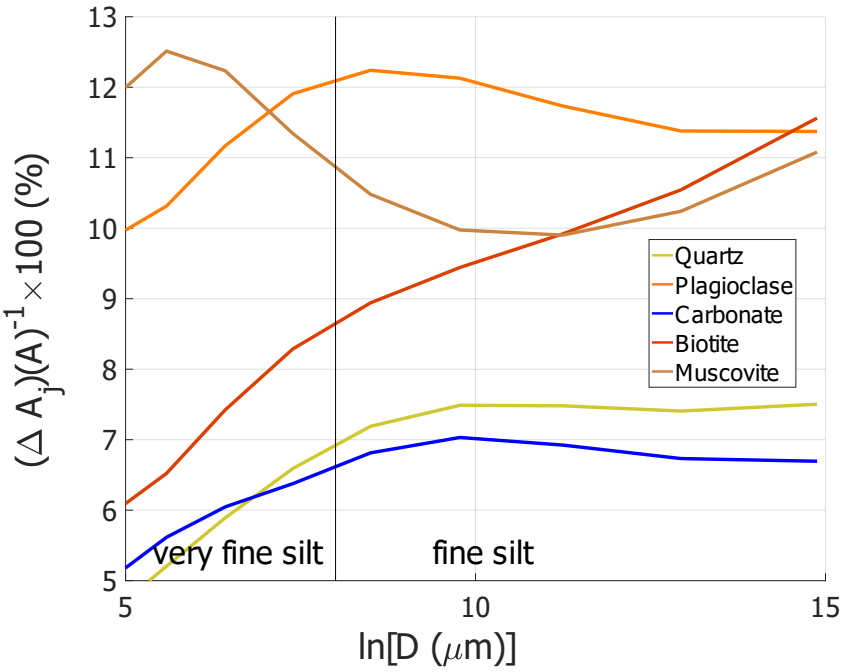

Figure 1.2: Simulation of changes in grain area. In addition to computing the perimeter of the convex hull, we use the Fourier smoothed perimeter, which is calibrated with Monte Carlo simulations of grain roughenss (Fig. 1.1). The change in area of the j^{th} mineral (ΔA_j) is normalized by the grain area A, which is assumed to by a circle of the equivalent diameter.

2 The embedded distribution

2.1 Methods

The embedded distribution takes on the form,

$$N^d_{j,k}(D_i) = \frac{N_{j,k,i}}{\sum_{i=k}^{i_{\max}} N_{j,k,i}}, \tag{2.1}$$

where the $N^d_{j,k}(D_i)$ distribution is measured for the j^{th} mineral at the k^{th} cluster size within the grain size D_i of the i^{th} size. The cluster-size distribution $N^c_j(D_k)$ can be written as the sum of the $i_{\max}-i+1$ discrete terms in the k^{th} $N^d_{j,k}(D_i)$ distribution as

$$N^c_j(D_k) = \sum_{k=i}^{i_{\max}} N^d_{j,k}(D_i). \tag{2.2}$$

We test the goodness-of-fit for the embedded distributions listed in the main text (log-Gaussian, Weibull, fractal and exponential), but given the additional complexity of the embedded distribution, we try to fit a two-term exponential ($y = a_1 e^{-a_2 D} + a_3 e^{-a_4 D}$), a two-term power law ($y = a_1 D^{-a_2} + a_3$) and a two-term Gaussian ($y = a_1 e^{\frac{-(D-a_2)^2}{a_3}} + a_4 e^{\frac{-(D-a_5)^2}{a_6}}$) with fits in linear and log space. Given that there can be few grains at the tail end of an $N^d_{j,k}(D_i)$ distribution, we truncate sizes larger than $i + 50$ for the purpose of fitting.

2.2 Results

In this section, we explore the extent to which clusters of a given size are distributed in grains of larger sizes, and discuss the best fit for this type of distribution. Each of the embedded $N^d_{j,k}(D_i)$ distributions for all minerals and all cluster sizes shows a rapid decay in cluster frequency as grain size increases, followed by an inflection point and a shoulder of the distribution (Fig. 2.1). Though some of the one-term distributions provide good fits, none capture the complexity present in the $N^d_{j,k}(D_i)$ distributions. The only two-term distributions to fit the peak and shoulder simultaneously for all minerals and all sizes are the two-term log-Gaussian and two-term Gaussian distributions (Fig. 2.1). Given that the distributions decay rapidly with size, the two-term Gaussian provides a comparable fit to the two-term log-Gaussian. For the two-term log-Gaussian, the frequency approaches zero at the largest sizes. This provides a poor fit at the tail end of the distribution (only seen in log–log space) because the data are discrete and take on only integer values, whereas continuous distributions can be infinitely small.

For all cluster-size distributions for all minerals, the smallest cluster size (two pixels) shows a distribution that intersects all other $N^d_{j,k}(D_i)$ distributions (red lines in Fig. 2.2), indicating a relatively high frequency at larger grain sizes. Two pixel clusters are in high abundance for both quartz and biotite across all grain sizes, but in much lower abundance in larger grains for muscovite and plagioclase. We observe a decrease in the frequency of small clusters in large grains going from rock fragments to sediment as each $N^d_{j,k}(D_i)$ distribution rotates to become more vertical. A vertical $N^d_{j,k}(D_i)$ distribution is associated with a narrow width for the first term, and indicates that clusters of a given size are much more likely to occur in grains of their own size than in grains of slightly larger sizes. This effect is most pronounced for quartz. Where the width of the $N^d_{j,k}(D_i)$ distribution is large for the first term (plagioclase with concave down $N^d_{j,k}(D_i)$ distributions), clusters of a given size are abundant in the next largest grain size, indicating that clusters are neighboured by single pixels of an adjoining mineral phase.

In analyzing how the parameters of the two term log-Gaussian are distributed as a function of cluster size (example shown for quartz in Fig. 2.3), the width of the first term decreases with cluster size for all minerals. This indicates that grains are increasingly more monomineralic as grain size decreases. None of the other parameters vary systematically across all minerals. By taking the ratio of the amplitude of the first two terms (terms shown individually for quartz in Fig. 2.3 and as a ratio for all minerals in Fig. 2.2), quartz has a much larger ratio than all other sediments, and quartz sediment has a much larger ratio than quartz rock fragments. For carbonate, biotite and muscovite, the ratio initially decreases with grain size, indicating a more monomineralic grain for small clusters. Plagioclase sediment shows a low ratio (~ 2) compared to other minerals for small cluster sizes, indicating that

small clusters are only twice as likely to be distributed in monomineralic grains than they are in grains of larger sizes.

2.3 Explanation for a two-term log-Gaussian embedded distribution

We infer that the breakdown of a grain is dependent on the exploitation of within-mineral versus mineral-boundary contacts. In this section we explore a third variable to explain mineral-contact strength and grain homogeneity, and use all three variables to explain the two-term Gaussian or log-Gaussian embedded distribution.

Given that the microfracture spacing is much smaller than the mineral/crystal size in rocks within our field area, the total extent of size reduction should depend primarily on within-mineral breakage. As a result, mineral hardness alone can be a good predictor of the area distribution of a mineral for sediment samples. A high dergree of within-mineral breakage can also explain why each mineral shows a much higher peak for the first term of the $N^d_{j,k}(D_i)$ distribution and a subdued peak for the second term. Substituting the log-normal and two-term log-normal distributions into the left and right hand sides of equation 2.2 leads to

$$A_1 e^{\frac{-(ln[D_k]-A_2)^2}{A_3}} = \sum_{k=i}^{i_{\max}} \left(a_{1,i} e^{\frac{-(ln[D_k]-a_{2,i})^2}{a_{3,i}}} + a_{4,i} e^{\frac{-(ln[D_k]-a_{5,i})^2}{a_{6,i}}} \right) \tag{2.3}$$

for the i^{th} parameters $a_{1,i}, a_{2,i} \cdots a_{6,i}$. Equations 2.3 could imply that the embedded distribution has to take on log-normal terms because the cluster size is log-normally distributed upon fragmentation. As shown in Fig. 2.2, parameters appear to vary systematically, especially for the first term. The functional form of the variation in parameters should be constrained to satisfy equation 2.3. Alternatively, an underlying log-normal distribution of the microfracture spacing within the bedrock might independently cause the cluster size and embedded distributions to be composed of log-normal terms. Further work would need to be done to determine whether the left hand side of equation 2.3 must be strictly satisfied by a two-term log-normal distribution, or if another family of distributions with a flexible range of parameters could lead to log-normality. This assertion might be valid where the mineral/crystal size and microfracture spacing are not distributed in the same way (e.g. one being log-normal and the other being fractal).

The $N^d_{j,k}(D_i)$ distribution describes how mineral clusters of a given size are distributed throughout larger grains. We suggest that there are three predominant factors with overlapping controls on each of the two terms of the $N^d_{j,k}(D_i)$ distribution. The first term describes the extent to which a cluster concentrates its size into grains that are equal to or only slightly larger than the cluster size. The first term is often very peaked for small cluster sizes of all minerals, indicating a high presence of monomineralic grains. The second term appears to describe the extent to which a cluster is distributed amongst much larger sizes. If only the first term were present, then the distribution would rapidly decay (approximately exponentially near the tail), and small clusters would not be observed in grains much larger than the cluster size. Parameters of the first peak therefore depend primarily on the extent of within-mineral breakage, and to a lesser extent on mineral-boundary breakage at grain sizes close to the cluster size.

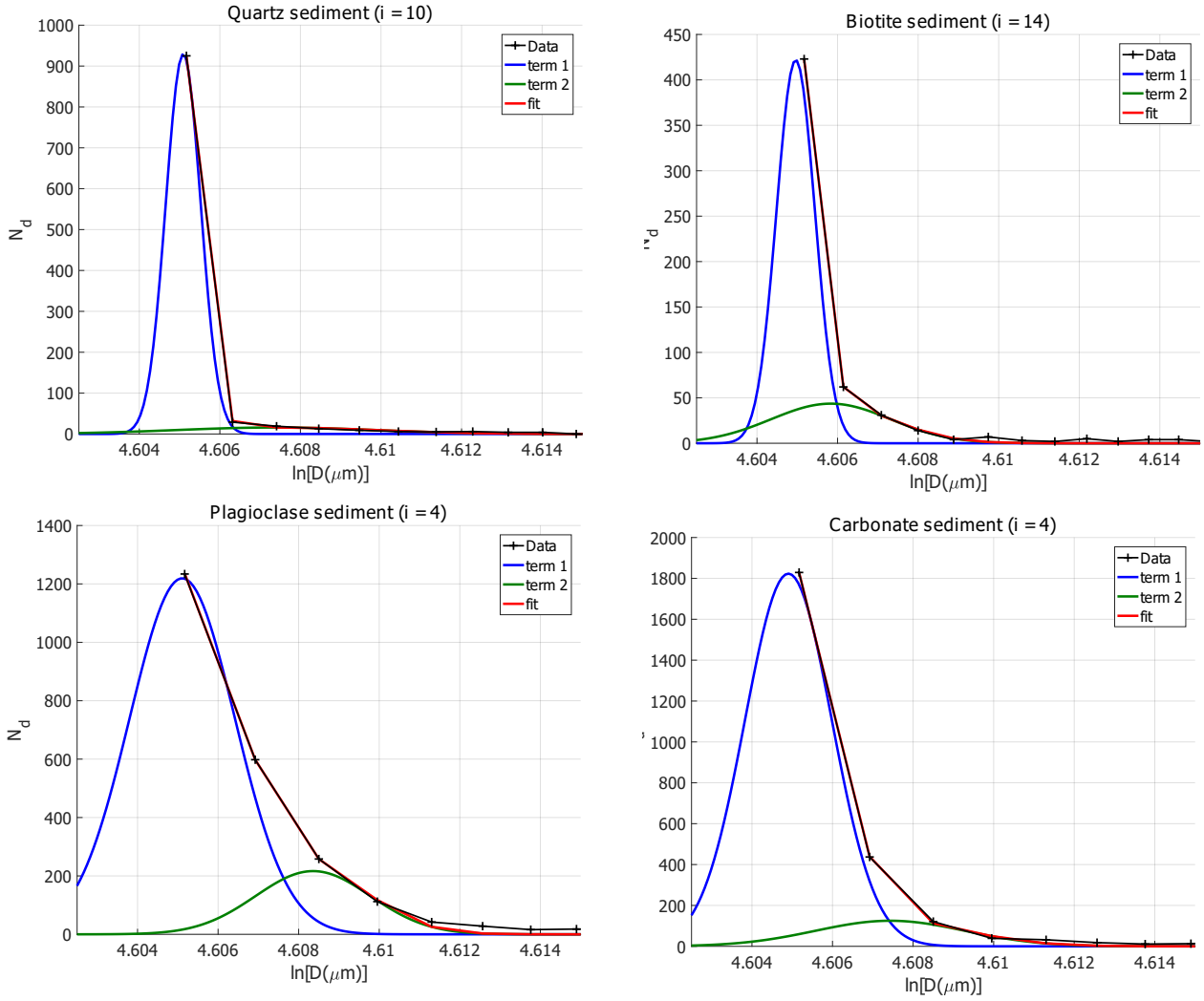

Figure 2.1: Examples of fitting a two-term log-Gaussian to the *ith* N_d distribution for metasedimentary sediment for quartz ($i = 10$), biotite ($i = 14$), plagioclase ($i = 4$) and calcite ($i = 4$). Data for the N_d distributions are shown with cross hatched black lines. The non-linear least squares estimate shown in red based on the underlying distributions of the the first term (blue) and second term (green). Values on the abscissa are shown in the range of 4.6 because all sizes were centered on a mean grain size of 100μm, which helped improve the convergence of the regression model.

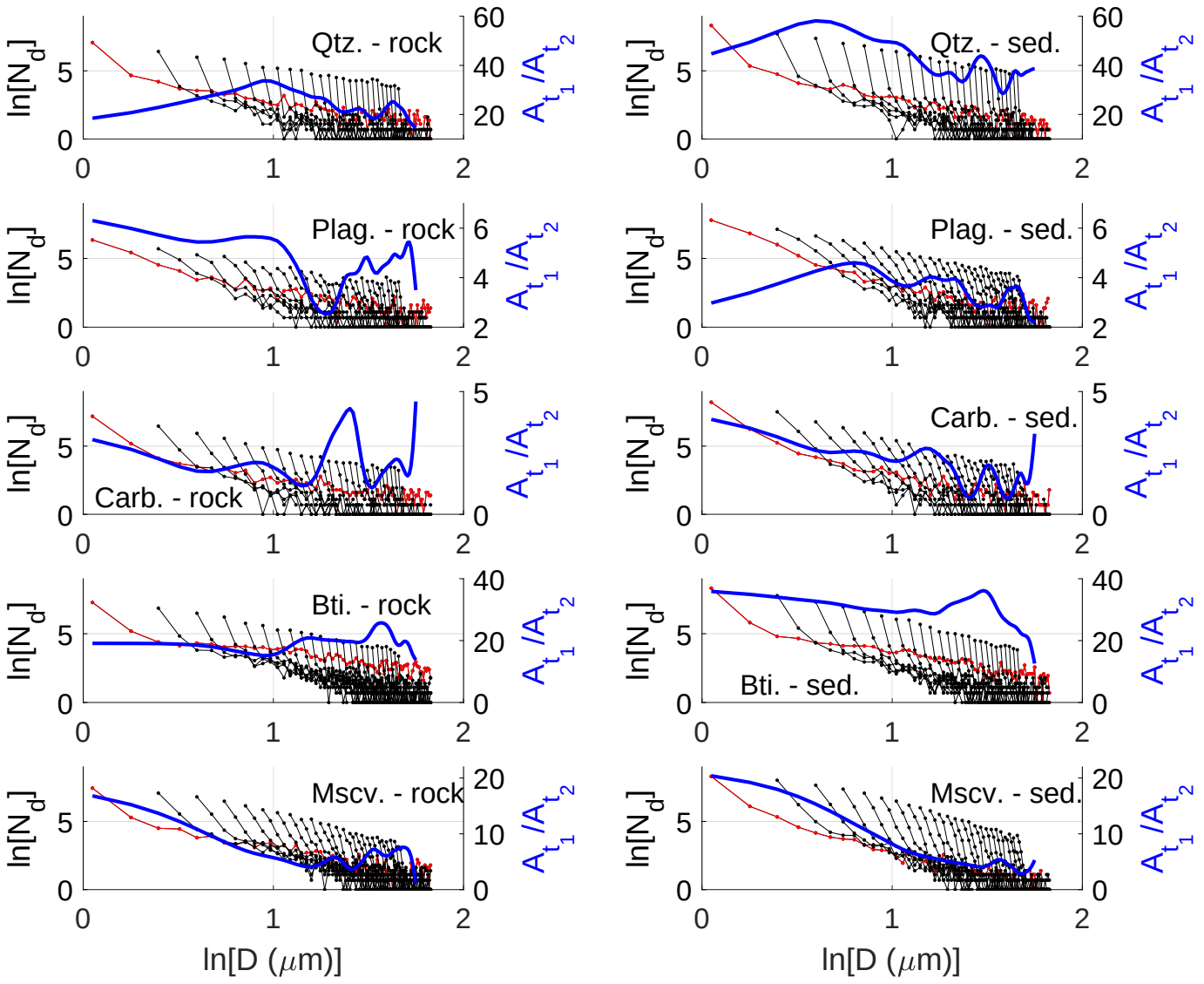

Figure 2.2: Embedded cluster size distributions N_d for rock fragments (left column) and sediment (right column). Every other i^{th} N_d distribution is shown with black dotted lines (left axis), with the exception of $N_d$at for $i = 1$, which is plotted in red so that it can be seen intersecting all larger N_d. Blue lines (right axis) show the ratio of amplitudes for the first (A_{t_1}) and second (A_{t_2}) terms interpolated by spline estimates (seen in Fig. 2.3).

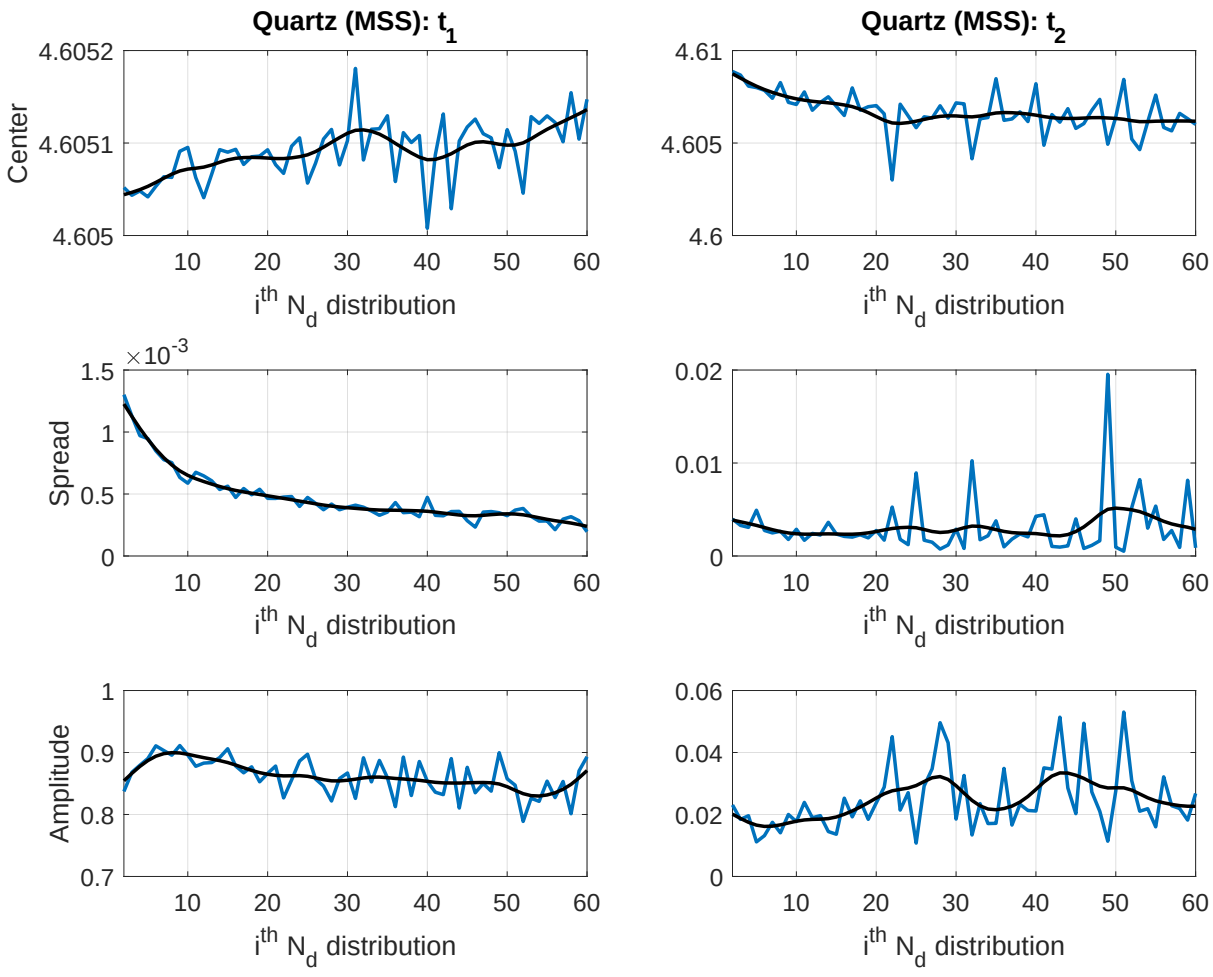

Figure 2.3: Estimates of parameters from the two-term log-Gaussian fits to the i^{th} N_d distribution for all metasedimentary quartz sediment grains. We only show the first $i = 60$ distributions. Parameter estimates of the first term (t_1) are shown in the left column and for the second term (t_2) in the right column. Values for the center and spread are taken from the sizes centered at $\ln[100 - D]$ (units in μm). The amplitudes are computed as the number of grains. We take a smoothing spline average across all sizes, and compute the ratio of spline estimates for the first and second term amplitudes (blue lines in Fig. 2.2)

.

We suggest that the stability of a grain also depends on the configuration of clusters within a grain, and the resulting distribution of internal stress. For example, plagioclase shows a high intragranular strength for small grains, whereby small clusters of plagioclase can be frequently embedded in much larger grains as shown by the low ratio of amplitudes between the two terms. In summary, parameters of the first term are primarily dependent on within-mineral strength, and to a lesser degree on the mineral-boundary strength. Parameters of the second term are controlled by the mineral-boundary strength for small grains, and for larger grains, on the distribution of internal stress as a function of the configuration of embedded minerals.

3 Grain size distributions of till samples

Twenty two till samples were collected from the terminus of 17 glaciers. Samples were collected from exposed cut banks where subglacial channels intersected the glacier terminus. Where the terminus could not be accessed, samples were collected from till in the forefield of the glacier. Samples were dry sieved to the smallest mesh size of 75 μm. Grain-size distributions are shown in Fig. 3.1.

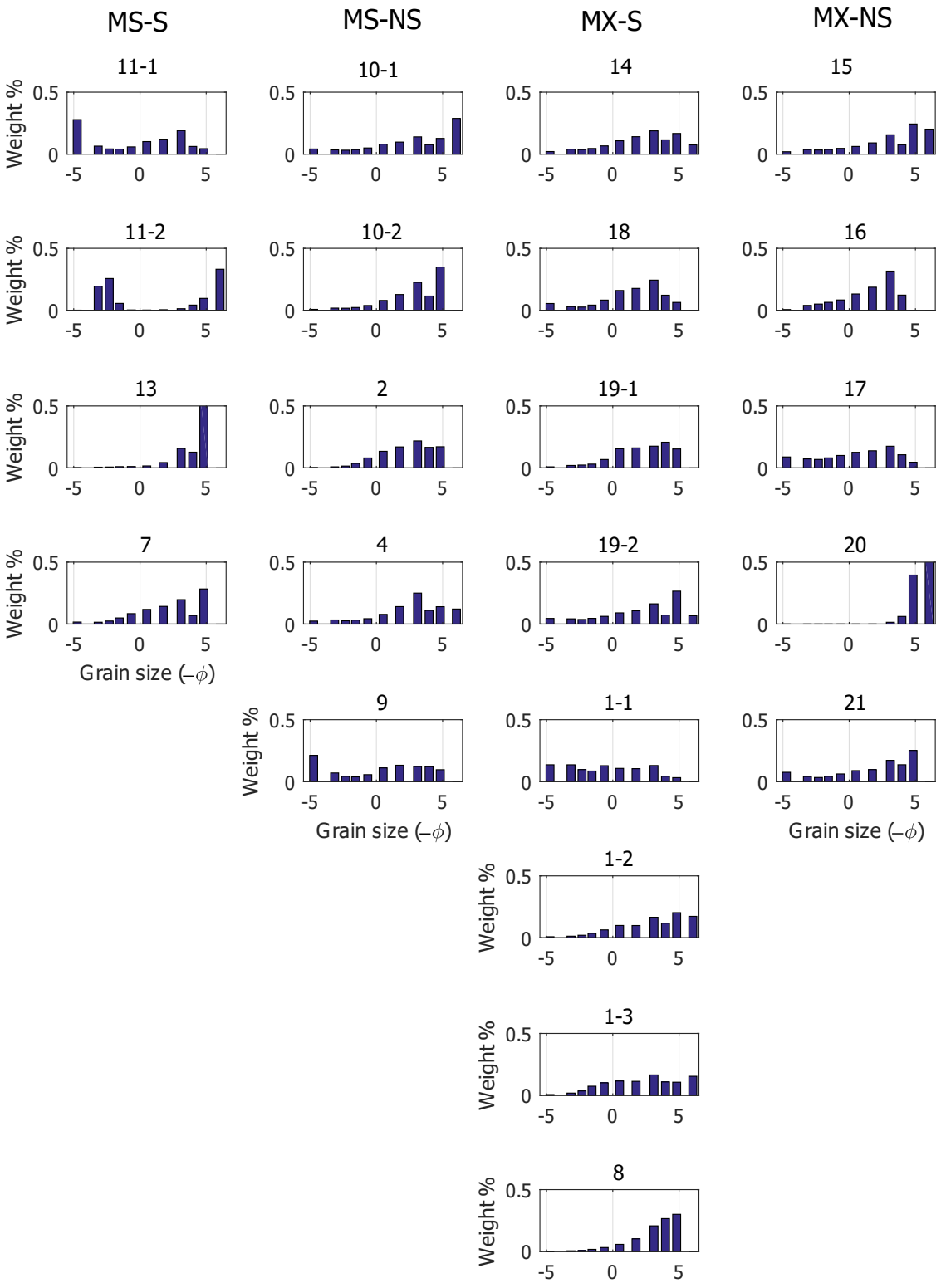

Figure 3.1: Grain-size distributions of till collected at the glacier terminus, with the glacier number labeled for each sample. Columns sorted by glacier type metasedimentary surge-type (MS-S), metasedimentary non-surge-type (MS-NS), mixed-lithology surge-type (MX-S) and mixed-lithology non-surge-type (MX-NS).

4 Estimates of erosion rates suspended sediment flux

In this section we describe the procedure for estimating an order-of-magnitude bedrock-equivalent erosion rate averaged over all glaciers in our field area. We measured a suspended sediment flux throughout the 2013 melt season at Glacier 1, and instantaneous suspended fluxes from all other glaciers in the study. To calculate an instantaneous suspended sediment flux from the measured sediment concentration, we carried out salt dilution gauging to quantify discharge. A more detailed description of sample collection and processing, as well as proglacial discharge and suspended sediment variability is given by Crompton and Flowers (2016).

Across all 20 glaciers, we find a linear relationship between discharge (Q) and sediment flux as SSF = $0.23\,\mathrm{Q}+0.51$. Most of the suspended sediment is smaller than medium silt, and the maximum measured grain size should be in suspension for the lowest measured discharge (Crompton and Flowers, 2016). We assume a diurnal proglacial discharge amplitude of $2\,\mathrm{m^3 s^{-1}}$ superimposed on sinusoidally varying discharge between May and October, such that the mean discharge at the beginning and end of the time series is zero, and the peak discharge of $4\,\mathrm{m^3 s^{-1}}$ occurs in the middle of the record. Assuming a mineral density of $2.5\,\mathrm{g\,cm^{-3}}$, the sediment mass integrated over one melt season is calculated to be $\sim 2 \times 10^7\,\mathrm{kg}$. Assuming a subglacial area similar to Glacier 1 of $5000\,\mathrm{m^2}$, this would correspond to roughly $1.5\,\mathrm{mm\,yr^{-1}}$ of bedrock erosion.

We can also derive a till deposition rate by assuming that the entire suspended sediment flux accounts for the fine grained material winnowed from till. We start by assuming that coarse grained material within till has a porosity of 0.15 (e.g. Fetter, 1980), and material smaller than fine silt is partially filling the coarse grained pore space and has a porosity of 0.5. By adding the contribution of the fine material that partially fills the voids of the coarse material, the total till porosity becomes 0.075. If we convert the porosity to an equivalent density, then we compute an aerially averaged till thickness of roughly $2\,\mathrm{cm\,yr^{-1}}$. These calculations do not account for the flux of bedload material, which we know to be significant in all streams.

5 Correlations between grain size and glacier dynamics

In this appendix section we discuss the influence of the relationship between grain size and surge-type glaciers. Crompton and Flowers (2016) show that sediments from non-surge-type glaciers overlying metasedimentary bedrock (MS-NS group) have a lower mean grain size than sediments from surge-type glaciers also overlying metasedimentary bedrock. Sediments from surge-type-glacier basins show no difference in grain size between mixed-lithology and metasedimentary basins. The correlation between surging and grain size initially motivated the reanalysis of these sediments using QEMSCAN. From this study, we confirm the correlation between grain size and glacier-type (with the exception of the Glacier 2 sample). The added result from this study is that we find no difference in mean grain size between MS sediment and MS rock fragments derived from surge-type versus non-surge-type basins. This result holds for pairwise comparison tests and tests of independent means. Furthermore, we cannot reject the null hypothesis that the mean difference in grain size between MS rock fragments from surge-type and non-surge-type basins is greater than zero.

Carrying out a PCA on the bulk mineralogy of metasedimentary rock samples shows that the first principal component can separate rocks from surge-type versus rocks from non-surge-type basins with minimal overlap between the two groups. This indicates that a linear combination of minerals in the bedrock is correlated to glacier-type. We hypothesize that the bedrock mineralogy is correlated with the macroscopic bedrock fracture spacing. The bedrock mineralogy likely has an influence on bedrock fracture spacing *and* on sediment size, but we expect that the bedrock fracture spacing is the dominant control on the distribution of surging glaciers in the Donjek Range (Crompton and others, 2018). The relationship between sediment size and glacier-type is therefore one of correlation with no causation in either direction, i.e. a lurking variable.

Bibliography

Crompton JW and Flowers GE (2016) Correlations of suspended sediment size with bedrock lithology and glacier dynamics. *Annals of Glaciology*, **57**(72), 142–150 (doi: 10.1017/aog.2016.6)

Crompton JW, Flowers GE and Stead D (2018) Bedrock fracture characteristics as a possible control on the distribution of surge-type glaciers. *Journal of Geophysical Research: Earth Surface*, **123**(5), 853–873 (doi: 10.1002/2017JF004505)

Dowdeswell JA (1982) Scanning electron micrographs of quartz sand grains from cold environments examined using Fourier shape analysis. *Journal of Sedimentary Research*, **52**(4), 1315–1323 (doi: 10.1306/212F812A-2B24-11D7-8648000102C1865D)

Fetter CW (1980) *Applied Hydrogeology*. Waveland Press

Gomez B, Dowdeswell JA and Sharp M (1988) Microstructural control of quartz sand grain shape and texture: implications for the discrimination of debris transport pathways through glaciers. *Sedimentary Geology*, **57**(1-2), 119–129 (doi: 10.1016/0037-0738(88)90021-8)

Mazzullo J and Ritter C (1991) Influence of sediment source on the shapes and surface textures of glacial quartz sand grains. *Geology*, **19**(4), 384–388 (doi: 10.1130/0091-7613(1991)019$(\$0384:IOSSOT$)\$2.3.CO;2)

Whalley WB (1978) An SEM examination of quartz grains from sub-glacial and associated environments and some methods for their characterization. *Scanning electron microscopy*, **1**, 353–360